Chapter 11
Dipole-Controlled Energy Level Alignment at Dielectric Interfaces in Organic Field-Effect Transistors

Philipp Stadler, Anna M. Track, Georg Koller, N. Serdar Sariciftci, and Michael G. Ramsey

Abstract In this section the energy level alignment at the semiconductor–dielectric interface in organic field-effect transistors is discussed. We focus at the comparison of pristine oxide structures with advanced organic interlayer structures. The interface is particularly interesting, since the performance of an organic field-effect transistor is significantly influenced by the energy level alignment. The study targets on an understanding of interfacial effects, hence complementary techniques are presented to investigate the interface. Most appropriately a combination of device analysis with a device-related photoemission spectroscopy study provides insight on the energy level alignment. Especially the role of commonly used organic interlayers is discussed, which enhance transistor performances. On organic–organic interfaces dipoles arise, which shift the relative positions of energy levels. Interestingly the magnitude and the direction of the shift is reflected in the device parameter analysis and in the corresponding photoemission spectra explaining the enhanced transistor performance.

11.1 Introduction

Organic field-effect transistors (OFETs) have gained a lot of interest in recent years for creating flexible, printable integrated circuits applying organic semiconductors [1–5]. The goal is to achieve high-performance device structures of organic

P. Stadler (✉) · N.S. Sariciftci
Physical Chemistry, Linz Institute for Organic Solar Cells (LIOS),
Johannes Kepler University of Linz, Altenbergerstrasse 69, 4040 Linz, Austria
e-mail: philipp.stadler@jku.at

A.M. Track · G. Koller · M.G. Ramsey
Surface and Interface Physics, Institute for Physics, Karl-Franzens University Graz,
Universitätsplatz 5, 8010 Graz, Austria

Present address:
A.M. Track
NXP Semiconductors Austria GmbH Styria, Mikronweg 1, 8101 Gratkorn, Austria

H. Sitter et al. (eds.), *Small Organic Molecules on Surfaces*,
Springer Series in Materials Science 173, DOI 10.1007/978-3-642-33848-9_11,

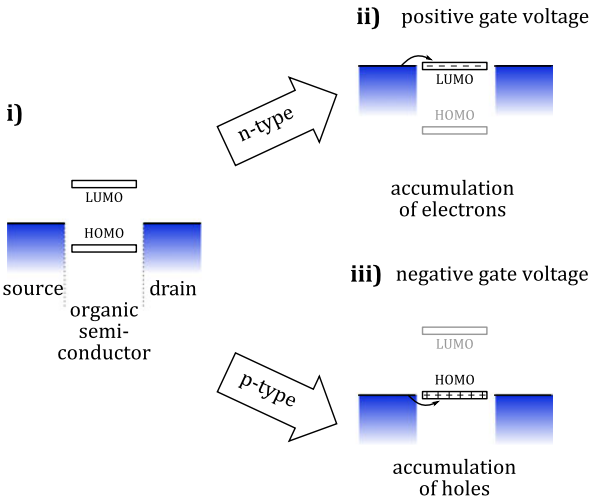

Fig. 11.1 Operation principle of OFETs depicted schematically in three stages: A conductive channel is formed by injecting charges (holes or electrons) to the initially intrinsic semiconductor as soon as a gate voltage is applied

field-effect transistors with operation frequencies in the MHz regime and low driving voltages between 1–10 V [6–8]. In state-of-the-art OFETs especially small π-conjugated molecules are performing well and a lot of optimized device structures are ready to take-off for integration in complex circuits [9, 10]. A closer look on the material aspect shows that organic small molecules have been optimized in terms of stability, their practical fabrication handling and their electrical properties such as morphology and charge carrier mobility [11, 12]. In previous chapters morphological issues have been addressed, especially the control of morphology is crucial for gaining high charge carrier mobilities for fast switching transistors [13–17]. Material research on dielectrics in OFETs is in progress as well. Field-effect devices require special dielectric materials, since they determine the magnitude of driving voltages, threshold voltages and limitations in switching speed [18, 19]. Ultra-thin dielectric layers exhibiting geometric capacitances in the range of several 100 nF cm^{-2} are nowadays implemented to OFETs [20–22]. In particular metal oxides are proven to be useful.

This review article addresses interfacial effects. Apart from the pure material aspects OFETs are sensitive to the nature of the interface between the organic semiconductor and the dielectric. They are interface-driven devices, where mutual effects arise, which significantly influence the formation of the conductive channel and hence the overall device performance [23, 24]. Differently to inorganic semiconductors, one has to consider that organic small molecules are initially intrinsic. Figure 11.1 depicts right the operation principle in OFETs: Depending on which type of semiconductor is used, either electrons (ii) or holes (iii) are injected and accumulated at the semiconductor–dielectric interface. Charge injection is precisely controlled by the electrical-field applied to the gate electrode. Thus organic transistors operate in an accumulation regime.

Obviously the nature of the interface between organic semiconductor and dielectric plays a major role for the charge transport. As a matter of fact the primary goal is

to design interfaces, where the energy level alignment is favorable for the formation of a conductive channel. Interestingly the combination of organic semiconductors with organic molecules leads to best performing transistors. The challenge is to understand the energy level alignment at organic–organic interfaces, which is profoundly discussed here. At least yet the golden rule for organics has not been found. In fact each family of organic semiconductor would behave different in combination with a certain dielectric surface.

11.2 Material and Structural Aspects in OFETs

In state-of-the-art OFETs usually hybrid or double layer dielectrics are applied [18, 19, 25]. Typical device structures are depicted in Fig. 11.2. Either silicon–silicondioxide or valve metals plus corresponding oxides lead to bottom-gated device structures.

The OFETs shown in Fig. 11.2, metal-oxide insulators are combined with thin, organic interlayers merging the advantages of different material classes. Metal oxides are nowadays implemented to inorganic norm integrated circuits e.g. MOSFETs and flash memory devices. Thin films in the range of 5–50 nm serve as excellent insulators with high breakdown fields (400–600 V μm^{-1}) and high dielectric constants ($\epsilon > 6$). In combination with organic interlayers hybrid systems enhance the mentioned interface properties. Their role is considered as a passivating layer removing charge carrier traps from the oxide surface. Especially pristine oxides exhibit a high

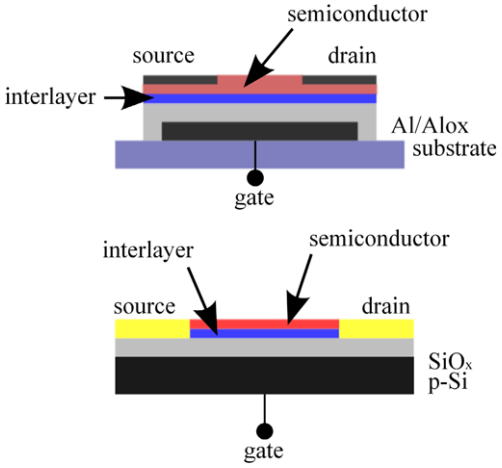

Fig. 11.2 Concepts used in literature of applied OFET structures. *Top*: Anodic grown oxide film on a valve metal (here aluminum) directly for a bottom-gate OFET structure. *Bottom*: Schematic of frequently adapted coplanar structured OFET using doped silicon as gate electrode (and as substrate) with thermally grown SiO_2 as insulator. Note in both cases the organic interlayer applied on top for a combined double layer or hybrid dielectric. The organic semiconductor is deposited on top of the interlayer forming a favorable interface. Figure courtesy of Stadler et al. [26]

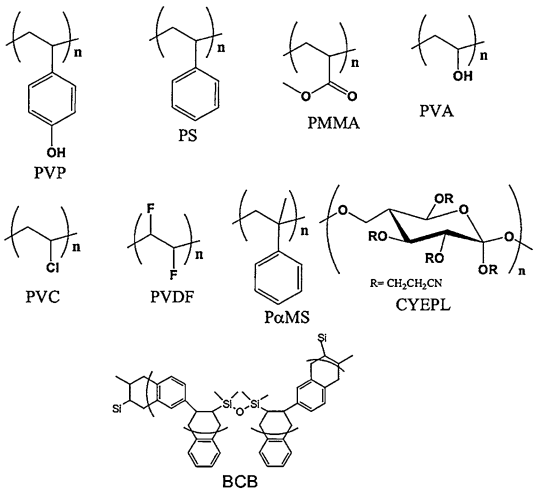

Fig. 11.3 Various polymers and resins used for high-performance OFETs. Figure courtesy of Singh et al. [28]

number of shallow traps, which interrupt the formation of a conductive channel [27]. The variety of organic material classes used as interlayers and active semiconductor layers opens almost an endless number of combinations.

The target is to find a matching organic–organic system, resulting in a systematic interface engineering [29–32]. However, empirical approaches to characterize interfaces are not sufficient, a deep understanding of organic–organic heterojunctions is required.

An excerpt of some typical, widely used examples for organic dielectric interlayer material classes, is suggested in the graphs below (Fig. 11.3). Classic polymers such as polystyrene (PS), bio-inspired polymers (Cypel) as well as molecular, cross-linkable resins (BCB) are implemented [33]. The latter class will be discussed in detail here in this review. An alternative approach to modify surfaces are covalently bonded functional molecules, which selectively attach to OH-terminated oxide surfaces and which form self-assembled monolayers (SAMs). Using the right surfactants surface properties can be changed for a more favorable alignment for the organic semiconductor. This technique reduces the organic interlayer to monolayers for ultra-thin devices. A number of candidates with different anchoring functional groups are shown in Fig. 11.4.

On the semiconductor side, typically molecules such as oligoacenes and oligothiophenes plus derivatives are used as hole-conductors (Fig. 11.5). Electron transport in systems with high electron affinity is found in fullerenes, functionalized perylenebisimides and perfluorinated π-conjugated molecules.

11.3 Organic Interlayers in OFETs

Zhang et al. [35] demonstrate with an empiric OFET study the influence of the organic interlayer on the device performance of OFETs. Systematically the impact of

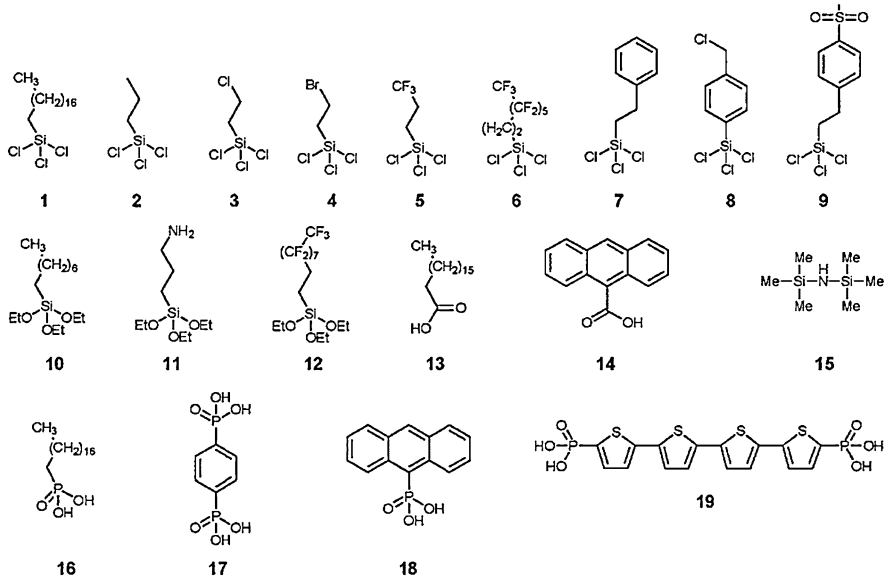

Fig. 11.4 Examples for SAM-molecules with different anchoring functionalized groups: Trichlorosilanes (*1–9*), triethoxysilanes (*10–12*), carboxylic acids (*13*,*14*), hexamethyl-disilazane (HMDS, *15*) and phosphonic acids (*16–19*). The most commonly used compound *1* is known as OTS (octadecyl-trichlorosilane). Figure courtesy of Miozzo et al. [19]

the organic interlayer on the performance has been studied by applying a structure as introduced in Fig. 11.2 (i). As seen in the Fig. 11.6 the current–voltage characteristics change significantly by varying the organic interlayer (T1–T4). The shape as well as the onset—the threshold voltage—are different for each interlayer. BCB (T1) exhibits the best performance, seen in graph (f). The question here arises: what is actually the driving force for the significant changes?

The system BCB–C_{60} turns out to perform very well when compared to other, widely used interlayers such as PMMA, PS or OTS. BCB used as organic interlayer enhances remarkably device performances of various n-type semiconductors [36–38]. Additional advantages for applying BCB are the thermal stability, which is in particular important for the growth of small molecules at higher temperatures beyond 100 °C, and the dielectric function, which remains constant over a wide frequency and temperature range [14]. Both characteristic properties can be read out from the graph presented in Fig. 11.7.

OFETs combining C_{60} with BCB have shown high mobilities and good performances in integrated circuits [6]. In addition, C_{60}'s unique symmetry and stability in ambient conditions allows probing with spectroscopic techniques. In the following we compare alumina and BCB as hybrid dielectric system. They have been widely used in organic electronics [2, 21, 36]. For a complementary study on the role of the BCB interlayer OFETs with and without the cross-linkable resin are character-

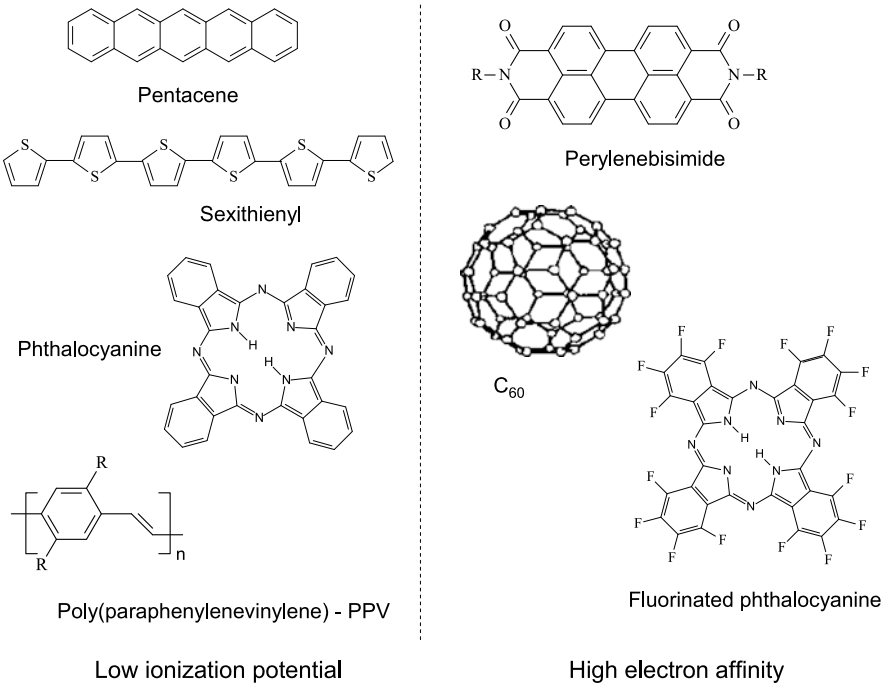

Fig. 11.5 Examples electron-dense organic p-type semiconductors (*left*) and electron-poor molecular systems for n-type transport. Figure courtesy of Cornil et al. [34]

ized. The corresponding device structures are depicted in Fig. 11.8, which serve as a model system discussed in the next chapter.

11.4 Threshold Voltage as Interface Parameter

In OFETs the threshold voltage represents *the* interface parameter per se. Hence for the threshold analysis the performance characteristics of both transistors with and without BCB is plotted in Fig. 11.9. The black line represents the device with BCB and the red line is assigned to the device without BCB. The onset in the current—the threshold—is actually shifted to higher voltages without BCB, seen in the linear plot in the inset. Consequently the latter structure operates at higher driving voltages, which acts as persistent burden. In addition by removing BCB the on/off ratio is reduced and hysteresis arises. All these issues are negative aspects in view of transistor circuit analysis.

A direct measure of the role of the interlayer in an OFET is consequently the threshold voltage U_{th}, which is considered as *the* interface parameter. Different groups have empirically proven influences of e.g. of the organic interlayer to the

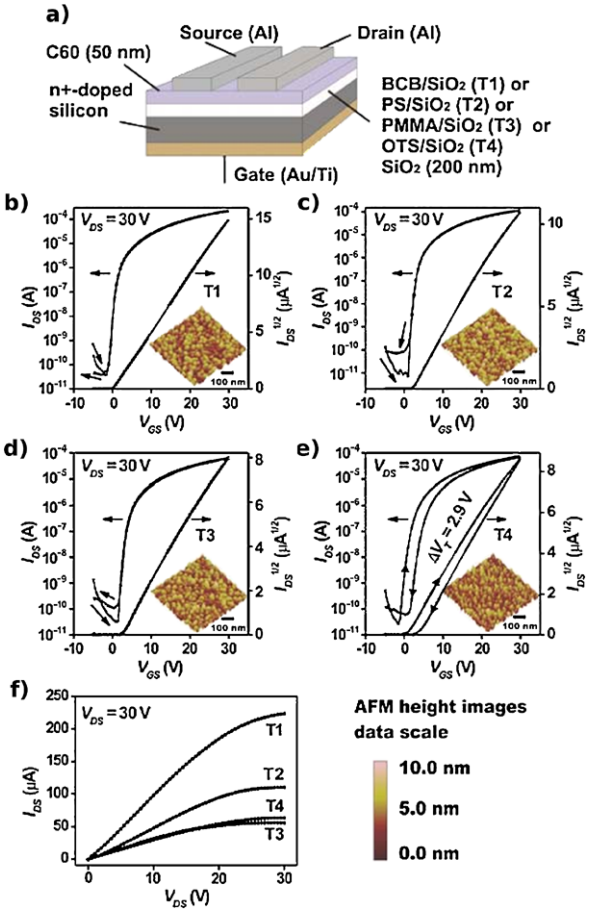

Fig. 11.6 Different current–voltage characteristics of C_{60}-based FET with four different interlayers. The device threshold and the absolute current value is influenced by the organic interlayer. Within the interlayers discussed here the combination BCB–C_{60} is obviously the best choice. Figure courtesy of Zhang et al. [35]

threshold voltages [27, 40–43]. The threshold voltage U_{th} represents by definition the gate voltage at which charge carriers are injected from the source electrode. In case of n-type organic semiconductors, the LUMO is then close to the Fermi potential of the electrode (Fig. 11.10).

The parameter extraction has to be performed with care, since OFETs often represent non-ideal systems. Contact resistances at the electrode–organic interface are influencing the source–drain characteristics and consequently the threshold voltage [44]. In order to work around these effects and for determining a reliable value for the onset in the transfer characteristics, the second derivative (SD) method is applied. The presented model system particularly exhibits low contact effects and optimized thin-film dielectrics, which itself approaches ideality [45–47]. A sketch in Fig. 11.11 below actually demonstrates an example for extraction. The threshold is defined at the inflection point in the transfer curve, which is read out from he second derivative. The plot exhibits then a maximum at the onset (indicated in the

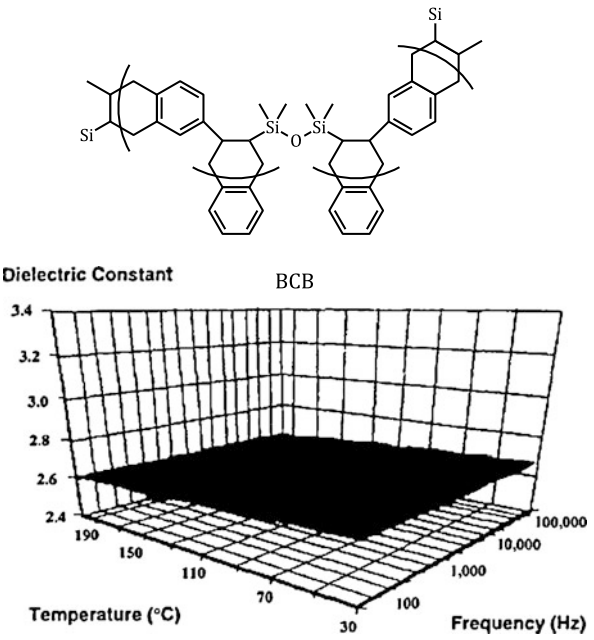

Fig. 11.7 *Top*: The structure of cross-linked benzocyclobutene derivative (Cyclotene, Dow Chemicals, $\epsilon = 2.6$) is shown. Underneath the dielectric function of a thin film is plotted as function of temperature and frequency. Figure courtesy of Mills et al. [39]

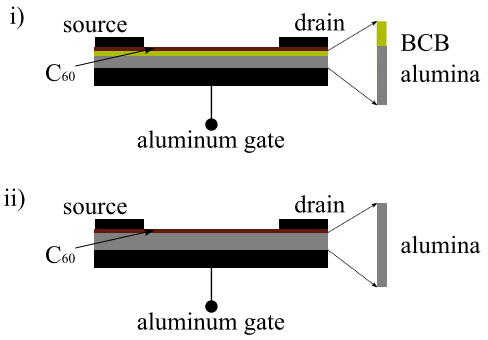

Fig. 11.8 Schematic of complementary model systems: C_{60}-based FET structures using hybrid dielectric with alumina/BCB (i) and pristine oxide (ii). Figure courtesy of Stadler et al. [26]

graph). The SD method has been derived from a MOSFET analysis [48]. However, its reliability has been demonstrated in OFET systems too [49].

Coming back to the initial Fig. 11.9 the threshold voltage is extracted from both curves. The result is plotted in Fig. 11.12, where the peak maximum is found at 0–0.1 V for the BCB device, whereas for the reference structure without BCB interlayer the maximum arises around 0.7 V. Obviously the shift in threshold voltage ΔU_{th} is 0.6 V, which is significant. It indicated that the energy levels at the interface align differently: BCB pushes the LUMO, already close to the Fermi level of the electrode, while on the pristine oxide a potential offset is found [50].

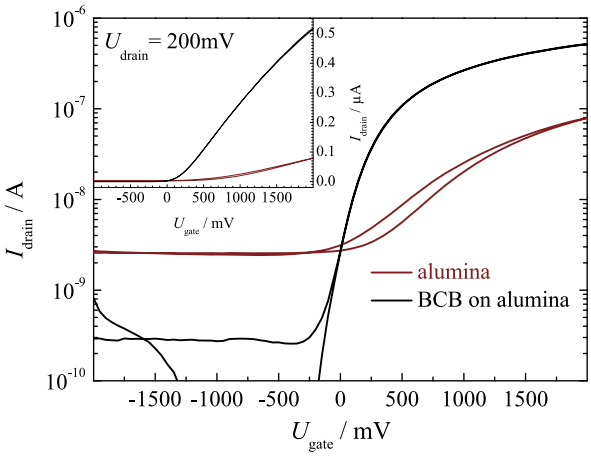

Fig. 11.9 Comparative OFET transfer characteristics with (*black*) and without (*red*) BCB in semilogarithmic and linear plot (*inset*). The performance drops in terms of lower on/off ratio, arising of hysteresis and apparently higher onset (threshold) for accumulation in case of missing BCB interlayer. Figure courtesy of Stadler et al. [26]

11.5 The Role of the Dielectric Interlayer in OFETs

Seen in the threshold voltage analysis the energy levels of the organic semiconductor at the interface is determined exclusively by the alignment at the interface. Thus the channel region in an OFET is reflected by a simple metal-insulator-semiconductor (MIS) structure. The gate electrode serves as a reference metal for the Fermi potential, followed by the insulator (hybrid dielectric) and the semiconductor. The energy diagram is depicted in Fig. 11.13, starting with the gate metal left-hand side followed by metal-oxide, organic interlayer and finally the organic semiconductor.

Indicated in the schematic pure material parameters are defined, such as the electron affinity (*EA*), the ionization potential (*IP*) and work functions ϕ of metals and metal oxide. Undefined parameters are actually found at interfaces, where the energy level alignment is controlled by dipoles [51–53]. They are indicated in the vacuum-level offset (Δ). The magnitude is determined by the nature of the interface. As shown in the diagram the role of the organic interlayers is assigned to tune energy levels of the semiconductor to more favorable positions compared to pristine oxide surfaces. This obviously happens, as indicated by the arrow in the

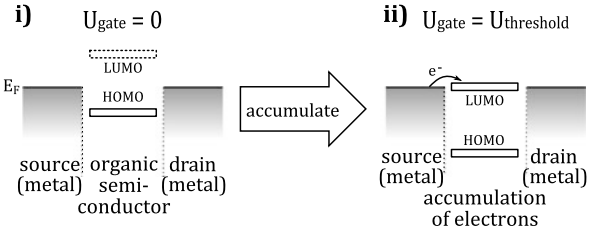

Fig. 11.10 (i) OFET at zero potential. The LUMO is indicated, the Fermi level for C_{60} is within the gap. In (ii) the situation is depicted after applying the threshold potential. Per definition now the LUMO converges the Fermi potential from the electrode. Charge injection from source is energetically enabled and the semiconductor can accumulate with electrons

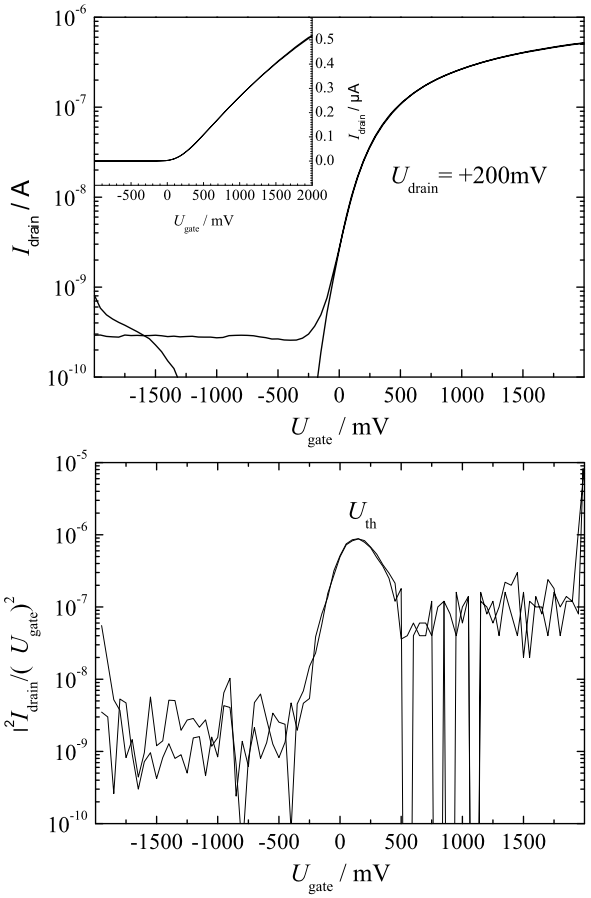

Fig. 11.11 Threshold voltage extraction applying the second derivative method. The *top graph* is the transfer characteristics, at the inflection point the second derivative (*bottom*) renders a maximum. The peak is a good estimate for the threshold voltage. Figure courtesy of Stadler et al. [26]

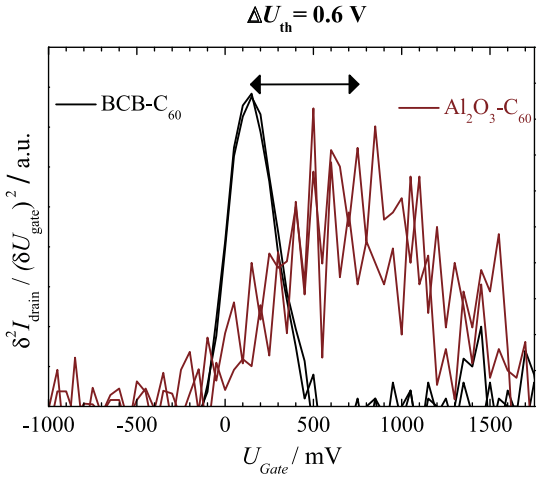

Fig. 11.12 Second derivative of plot in Fig. 11.9. The active role of the BCB is visible by the distinct shift of the peak maximum from around 0.7 V down to 0.1 V. Figure courtesy of Stadler et al. [26]

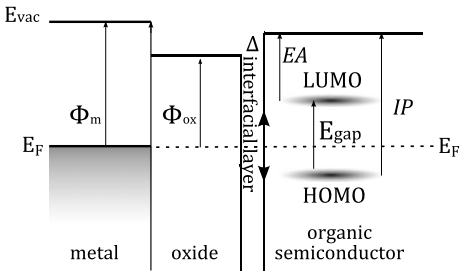

Fig. 11.13 Schematic energy diagram of an metal–insulator–semiconductor (MIS) structure with an organic interlayer between the metal–oxide and the organic semiconductors. The dipole controls the position relative to the gate metal. Figure courtesy of Stadler et al. [26]

schematic the interlayer either pushes HOMO or LUMO close to the Fermi level. Depending whether n-type or p-type organic semiconductors are used, the matching interlayer would drive the threshold voltage to a position close to the Fermi level. Consequently in ideal systems the threshold voltage should be close to 0 V. A good example for such a dipole-controlled alignment is seen in case of C_{60}–BCB, which obviously pushes the LUMO close to the Fermi potential visible in the threshold potential around 0 V.

11.6 Photoemission Spectroscopy on Transistor-Related Structure

In light of the energy diagram the substantial issue is now to seize origin and magnitude of dipoles at interfaces involving organic thin films. Here OFETs may only provide an indirect insight to interfaces, which can be shielded by parasitic, competitive device effects. There is need for a complementary technique, which provides direct access to interface properties. A solution is apparently to apply photoemission spectroscopy (PES).

The advantage is its surface sensitivity, which ranges between 10–30 Å, depending on the excitation source. Few layer films of organic π-conjugated small molecules actually correspond to the mean-free-path of electrons. In several contributions shown before growth and characterization of organic ultra-thin films is presented in great detail.

Device-related photoemission spectroscopy is particulary challenging, since layers cannot be directly grown in-situ in the PES vacuum system. BCB for instance is solution processed, alumina is grown electrochemically. For a cross-check a reference spectrum of C_{60}, which has been exposed to air (Fig. 11.14), is presented. As the UV-source He(I)-lamp excites at 21.2 eV, a heavy p-doped silicon(110) waver serves as reference substrate. The spectral features conform to literature data on in-situ deposited organic films [55]. The fingerprint DOS of C_{60} is clearly identified. The ionization potential *IP* of the thin solid film is determined at 6.5 eV [56], which is derived by adding the work function and the distance from the Fermi energy to the maximum of the HOMO. The corresponding energy levels are illustrated in the energy diagram in Fig. 11.15.

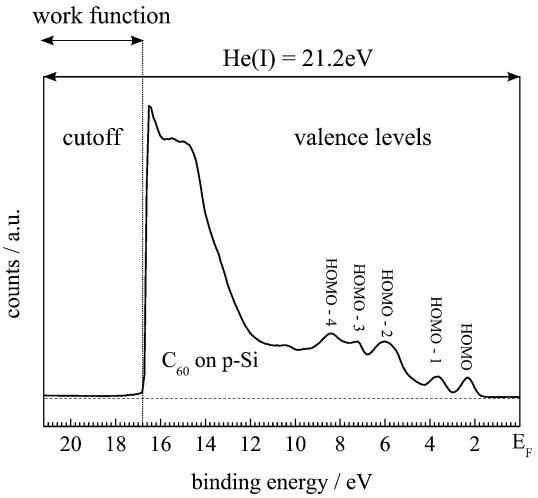

Fig. 11.14 UPS spectra of ex-situ vacuum-prepared C_{60} on p-Si. The DOS is identified and labeled in the graph. Their quality are comparable to in-situ vacuum-prepared samples from e.g. Sakamoto et al. [54]. Valence levels and work function obtained by a metal substrate as well as the excitation energy are indicated. Figure courtesy of Stadler et al. [26]

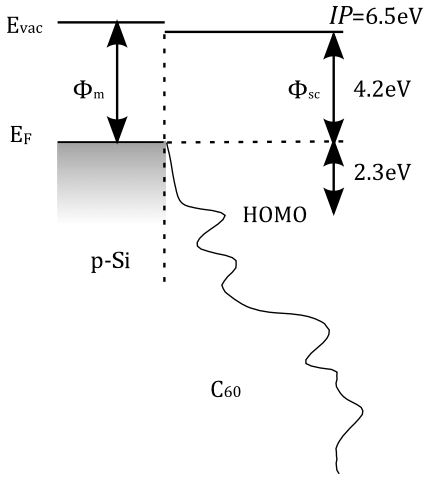

Fig. 11.15 Energy diagram of p-Si-C_{60} structure. From the peak of the HOMO to the vacuum level the ionization potential *IP* is derived. The HOMO actually is found 2.3 eV below the Fermi edge. Figure courtesy of Stadler et al. [26]

Instead of well-defined substrates the uppermost layer of C_{60} has to be probed in an adopted OFET channel for the desired interface study. The source–drain electrodes are not needed, a simple MIS structure with ultra-thin C_{60} models the channel in the corresponding OFET structure, see Fig. 11.16. As substrates aluminum-alumina w/o BCB is applied. A cross-section of the discussed sample is depicted in Fig. 11.17 revealing the investigated interface: alumina–BCB and BCB–C_{60}. Almost the shape of the fullerene molecule is visible in the electron transmission.

A direct comparison of samples with and without BCB are directly investigated applying PES. Now the valence levels (0–8 eV BE) and the electron cut-off (16–21.2 eV BE) are plotted in Fig. 11.18. Qualitatively minor changes are observed. The features in the valence levels are smeared out a bit on alumina, on BCB they

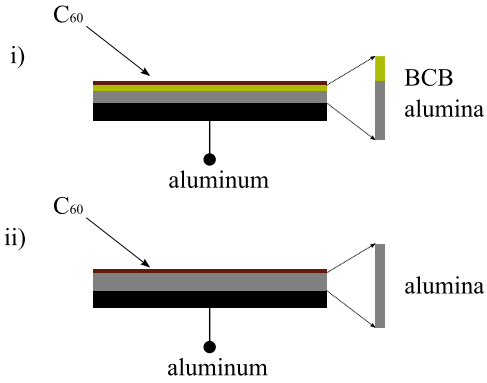

Fig. 11.16 Sample structure for device-related PES. The role of BCB is investigated by copying the transistor structure from Fig. 11.8 without source–drain contacts

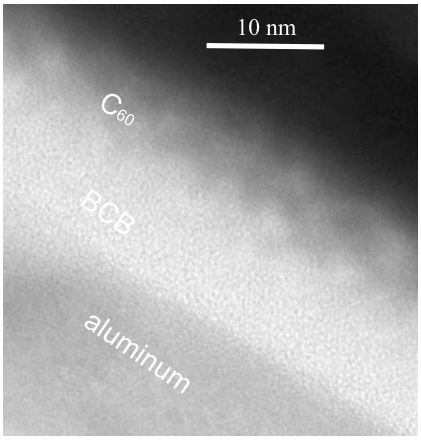

Fig. 11.17 Corresponding TEM picture of thin C_{60} layer on BCB from Fig. 11.16 (i). The TEM cross-section resolves the interfaces of fullerene–BCB and BCB–alumina. Note the thickness indicated by the *scale*. The C_{60} layer diameter is 20–30 Å within the discussed sensitivity range of the PES experiment. Figure courtesy of Stadler et al. [26]

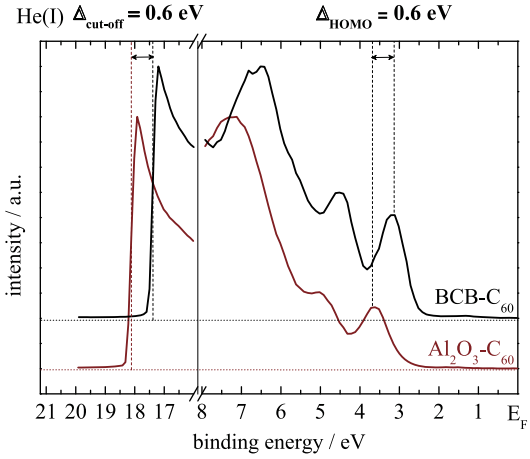

Fig. 11.18 Spectra revealing the DOS of C_{60} on BCB (*black line*) and pristine alumina (Al_2O_3, *red line*). The features are well defined. A dipole by 0.6 eV controls the position of the entire spectrum relative to the gate reference metal (E_F). Figure courtesy of Stadler et al. [50]

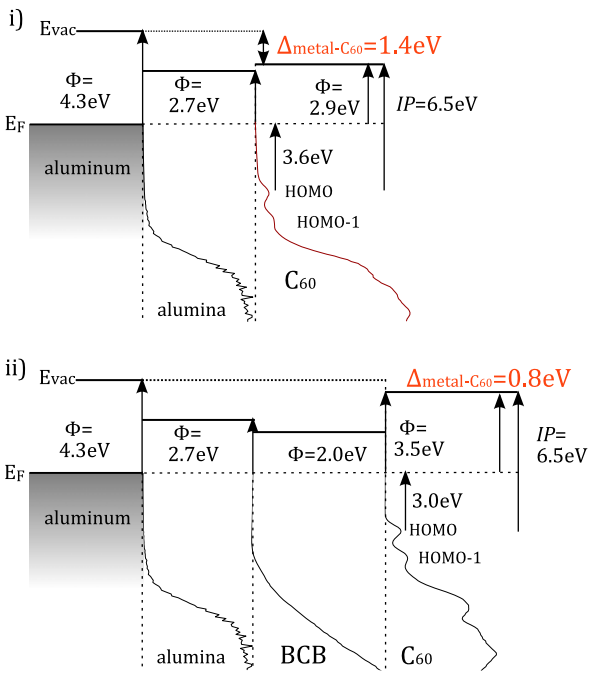

Fig. 11.19 Energy diagram of alumina–C_{60} and alumina–BCB–C_{60} as measured by PES. Note that all DOS spectra are experimental results by a careful layer-by-layer analysis. As indicated BCB actually shifts C_{60} levels upwards back to a situation as found at e.g. p-Si 11.14. The dipole at the organic–organic interface is reduced, compared to the offset between metal–C_{60} the valence levels differ by 0.6 eV. Figure courtesy of Stadler et al. [26]

are better defined. Anyhow these effects are almost negligible compared to the significant change induced by BCB. The entire spectrum shifts by 0.6 eV towards the Fermi energy. The changes are concomitantly found for the valence features as well as for low kinetic energy electrons in the cut-off and seen identically in the threshold analysis in Fig. 11.12 before.

The energy level analysis is completed by measuring all interfaces involved, starting with alumina, BCB and finally C_{60}. The results are illustrated in the MIS energy diagram, all values are gained from the device-related PES. As discussed earlier the valence levels of each component are measured, the energy offset shows a significant drop in the vacuum level for aluminum–C_{60} in the structure without BCB interlayer. The dipole Δ is labeled in Fig. 11.19. Interestingly at the oxide–organic semiconductor interface the vacuum levels align, which leads finally to the huge potential drop from C_{60} to the reference metal of 1.4 eV. The changes induced by the BCB unveil the role of BCB, seen in Fig. 11.19, where actually a dipole-controlled alignment is found. Compared to the oxide–organic interface the energy offset is huge, but consequently the potential drop with respect to the metal is decreased by 0.6 eV (marked red in the graph). The basic role of BCB is to shift the relative position of the C_{60}-DOS with respect to gate. Both PES and threshold voltage shift are in good agreement reducing the dipole (and voltage) by 0.6 eV (or V). The role of the organic interlayer is to compensate the disadvantageous vacuum-level offset formed on the pristine oxide structure. It re-establishes the situation found for the case with p-Si and C_{60}.

11.7 Discussion

Both results, OFETs threshold voltage and transistor-related PES experiment demonstrate a complementary technique to understand organic interfaces. The role of organic interlayers in OFETs is interpreted to be more than just a passivation layer. In fact the results show that an organic interlayer changes the energy level alignment of the corresponding organic semiconductor significantly. The experiments point out their inherent *active* role.

Instead of vacuum-level alignment a dipole is formed at the organic–organic interface, which finally drives the energy levels of the organic semiconductor to a position close to the Fermi level. The built-in potential is to some extend compensated. A similar alignment is for instance found on metals or silicon substrates [54, 55, 57]. Though the model system BCB–C_{60} studied in detail here does not represent organic interfaces in general, the aspect of dipole-controlled alignment is widely accepted in the literature [58]. Organic interface dipoles can be significant, and in light of the complementary OFET results, a shift by 0.6 V as detected for BCB has a deep impact on the device performance. Hence a lot of attention has recently been paid to interface engineering with organic interlayers in organic electronics device studies. A closer look to the oxide-only structure allows a number of conclusions as well. On the contrary to BCB, on pristine alumina rather vacuum-level alignment is found, at least the energy offset at the interface is low compared to the organic–organic system. Consequently the energy drop found between metal–metal oxide is passed on to the organic semiconductor leading finally to a large offset in the vacuum level by 1.4 eV. In the field-effect transistor the offset is then revealed by the increased threshold voltage, since the inherent built-in potential can only be compensated by applying gate voltage. Similar effects have been presented for a number of pristine oxide OFET structures, where significant threshold potentials arise [27]. These support the assumption of a vacuum-level alignment on oxide–organic semiconductor interfaces.

11.8 Conclusion and Outlook

A sound theory on organic interlayer's relating their magnitudes of introduced dipoles and their influence on device performances is yet not found. Most of commonly used interlayers are presented in rather empirical studies. In various contributions interface effects on device performances are reduced to surface traps or surface passivation. The authors believe that such consideration are in agreement with the dipole-controlled alignment uncovered by a device-related photoemission study. Pristine oxide surfaces due to OH-termination indeed introduce trapped states in the organic semiconductors. Negative charges at the interface are present, which push the energy levels of the semiconductor downwards and away from the Fermi energy. In OFETs they have to be compensated by the gate voltage, thus leading

to increased and unwanted threshold potentials. Device-related photoemission can help to understand the interaction at organic–organic interfaces. Still suspense as regards the magnitude and polarity of the dipole is a real problem. An approach to model and systematically analyze organic interfaces might be derived from donor–acceptor studies in bulk-heterojunction solar cells [59, 60]. Depending on the system the interlayer either acts as quasi-donor or acceptor, which becomes apparent by the threshold voltage. At least from the experimental data, the dipoles formed at heterojunctions are similar to interactions on π-conjugated systems. Therefore interface studies could be expanded for photo-induced effects on OFET interfaces for a better understanding.

11.9 Summary

The contribution discusses the complex nature of organic interfaces, which are key-components in organic electronic devices. Especially in OFETs the formation of a conductive channel is sensitive to mutual, interfacial effects. The variety of organic interfacial or dielectric layers has increased during the past years, at the same time the development of small π-conjugated molecules has yielded in an enormous amount of systems. Practically a number of combinations result in good performing organic field-effect transistors, which in the end will be implemented to complex, organic integrated circuits.

In this article interfacial effect in view of the complex energy level alignment is investigated. The question arises of why organic interlayers enhance transistor performances compared to devices with pristine oxide. For gaining information about energy levels at the interface, complementary techniques are applied, one based on a systematic analysis of the threshold voltages in OFETs, one involving device-related photoemission spectroscopy. In detail, an oxide–organic interface is compared to an organic–organic interface using the model system alumina–C_{60} and BCB–C_{60}. The device analysis show clear results from both interfaces: as soon as BCB is applied, the threshold voltage is lowered from previous 0.7 V almost to 0 V.

A similar effect is found for the complementary photoemission study, where actually BCB induces a shift in the same magnitude resulting in a different energy level alignment at the interface. Interestingly the entire spectrum is shifted concomitantly, both valence features and secondary electron cut-off exhibit the same result. The quality of the spectra is not affected by the different interfaces.

The spectral data together with the device parameters provide valuable information about the organic–organic and the organic–oxide system. On the one hand, huge dipoles control the energy level alignment at the interface. They compensate built-in fields and consequently move valence levels to more favorable positions for creating a conducting channel in the OFET. On the other hand, at oxide–organic interfaces almost vacuum-level alignment is observed, therefore the compensation

of built-in fields has to be performed by applying gate voltage resulting in the disadvantageous huge threshold potential. Similar effects on oxide–organic interfaces have been reported by several groups in the literature. The authors believe that exactly the findings presented here can help to understand organic interface system and to tailor organic electronic devices to higher performances.

Still little is known about the energy level alignment at organic–organic interfaces. From empirical studies general pathways for high-performance systems have been demonstrated, and parameters are defined which may be considered for further development.

References

1. H. Klauk, U. Zschieschang, J. Pflaum, M. Halik, Ultralow-power organic complementary circuits. Nature **445**(7129), 745–748 (2007). doi:10.1038/nature05533. http://www.ncbi.nlm.nih.gov/pubmed/17301788
2. H. Klauk, U. Zschieschang, M. Halik, Low-voltage organic thin-film transistors with large transconductance. J. Appl. Phys. **102**(7), 074514 (2007). doi:10.1063/1.2794702. http://link.aip.org/link/JAPIAU/v102/i7/p074514/s1&Agg=doi
3. K. Myny, S. Steudel, S. Smout, P. Vicca, F. Furthner, B. van der Putten, a.K. Tripathi, G.H. Gelinck, J. Genoe, W. Dehaene, Organic RFID transponder chip with data rate compatible with electronic product coding. Org. Electron. **11**(7), 1176–1179 (2010). doi:10.1016/j.orgel.2010.04.013. http://linkinghub.elsevier.com/retrieve/pii/S1566119910001308
4. K. Suganuma, S. Watanabe, T. Gotou, K. Ueno, Fabrication of transparent and flexible organic field-effect transistors with solution-processed graphene source–drain and gate electrodes. Appl. Phys. Express **4**(2), 021603 (2011). doi:10.1143/APEX.4.021603. http://apex.jsap.jp/link?APEX/4/021603/
5. T. Sekitani, T. Someya, Stretchable, large-area organic electronics. Adv. Mater. **22**(20), 2228–2246 (2010). doi:10.1002/adma.200904054. http://www.ncbi.nlm.nih.gov/pubmed/20229571
6. T.D. Anthopoulos, T.B. Singh, N. Marjanovic, N.S. Sariciftci, A. Montaigne Ramil, H. Sitter, M. Coelle, D.M. de Leeuw, High performance n-channel organic field-effect transistors and ring oscillators based on C60 fullerene films. Appl. Phys. Lett. **89**(21), 213504 (2006). doi:10.1063/1.2387892. http://link.aip.org/link/APPLAB/v89/i21/p213504/s1&Agg=doi
7. T. Yokota, T. Nakagawa, T. Sekitani, Y. Noguchi, K. Fukuda, U. Zschieschang, H. Klauk, K. Takeuchi, M. Takamiya, T. Sakurai, T. Someya, Control of threshold voltage in low-voltage organic complementary inverter circuits with floating gate structures. Appl. Phys. Lett. **98**(19), 193302 (2011). doi:10.1063/1.3589967. http://link.aip.org/link/APPLAB/v98/i19/p193302/s1&Agg=doi
8. T. Sekitani, T. Yokota, U. Zschieschang, H. Klauk, S. Bauer, K. Takeuchi, M. Takamiya, T. Sakurai, T. Someya, Organic nonvolatile memory transistors for flexible sensor arrays. Science **326**(5959), 1516–1519 (2009). doi:10.1126/science.1179963. http://www.ncbi.nlm.nih.gov/pubmed/20007895
9. J.C. Ribierre, K. Takaishi, T. Muto, T. Aoyama, Flexible organic field-effect transistors and complementary inverters based on a solution-processable quinoidal oligothiophene derivative. Opt. Mater. **33**(9), 1415–1418 (2011). doi:10.1016/j.optmat.2011.03.015. http://linkinghub.elsevier.com/retrieve/pii/S0925346711001364
10. U. Zschieschang, F. Ante, T. Yamamoto, K. Takimiya, H. Kuwabara, M. Ikeda, T. Sekitani, T. Someya, K. Kern, H. Klauk, Flexible low-voltage organic transistors and circuits based on a high-mobility organic semiconductor with good air stability. Adv. Mater. **22**(9), 982–985 (2010). doi:10.1002/adma.200902740. http://www.ncbi.nlm.nih.gov/pubmed/20217824

11. T. Sakanoue, M. Yahiro, C. Adachi, H. Uchiuzou, T. Takahashi, A. Toshimitsu, Ambipolar light-emitting organic field-effect transistors using a wide-band-gap blue-emitting small molecule. Appl. Phys. Lett. **90**(17), 171118 (2007). doi:10.1063/1.2734389. http://link.aip.org/link/APPLAB/v90/i17/p171118/s1&Agg=doi
12. A. Huebler, F. Doetz, H. Kempa, H.E. Katz, M. Bartzsch, N. Brandt, I. Hennig, U. Fuegmann, S. Vaidyanathan, J. Granstrom, Ring oscillator fabricated completely by means of mass-printing technologies. Org. Electron. **8**(5), 480–486 (2007). doi:10.1016/j.orgel.2007.02.009. http://linkinghub.elsevier.com/retrieve/pii/S1566119907000365
13. M. Mas-Torrent, C. Rovira, Novel small molecules for organic field-effect transistors: towards processability and high performance. Chem. Soc. Rev. **37**(4), 827–838 (2008). doi:10.1039/b614393h. http://www.ncbi.nlm.nih.gov/pubmed/18362986
14. M. Ullah, I.I. Fishchuk, A. Kadashchuk, P. Stadler, A. Pivrikas, C. Simbrunner, V.N. Poroshin, N.S. Sariciftci, H. Sitter, Dependence of Meyer Neldel energy on energetic disorder in organic field effect transistors. Appl. Phys. Lett. **96**(21), 213306 (2010). doi:10.1063/1.3435477. http://link.aip.org/link/APPLAB/v96/i21/p213306/s1&Agg=doi
15. M. Ullah, A. Pivrikas, I.I. Fishchuk, A. Kadashchuk, P. Stadler, C. Simbrunner, N.S. Sariciftci, H. Sitter, Effect of source–drain electric field on the Meyer–Neldel energy in organic field effect transistors. Appl. Phys. Lett. **98**(22), 223301 (2011). doi:10.1063/1.3584131. http://link.aip.org/link/APPLAB/v98/i22/p223301/s1&Agg=doi
16. A. Pivrikas, M. Ullah, H. Sitter, N.S. Sariciftci, Electric field dependent activation energy of electron transport in fullerene diodes and field effect transistors: Gill's law. Appl. Phys. Lett. **98**(9), 092114 (2011). doi:10.1063/1.3557503. http://link.aip.org/link/APPLAB/v98/i9/p092114/s1&Agg=doi
17. A. Pivrikas, M. Ullah, T.B. Singh, C. Simbrunner, G.J. Matt, H. Sitter, N.S. Sariciftci, Meyer–Neldel rule for charge carrier transport in fullerene devices: a comparative study. Org. Electron. **12**(1), 161–168 (2011). doi:10.1016/j.orgel.2010.10.014. http://linkinghub.elsevier.com/retrieve/pii/S1566119910003393
18. Y.M. Park, J. Daniel, M. Heeney, A. Salleo, Room-temperature fabrication of ultrathin oxide gate dielectrics for low-voltage operation of organic field-effect transistors. Adv. Mater. **23**(8), 971–974 (2011). doi:10.1002/adma.201003641. http://www.ncbi.nlm.nih.gov/pubmed/21341309
19. L. Miozzo, A. Yassar, G. Horowitz, Surface engineering for high performance organic electronic devices: the chemical approach. J. Mater. Chem. **20**(13), 2513 (2010). doi:10.1039/b922385a
20. H. Klauk, M. Halik, U. Zschieschang, F. Eder, D. Rohde, G. Schmid, C. Dehm, Flexible organic complementary circuits. IEEE Trans. Electron Devices **52**(4), 618–622 (2005). doi:10.1109/TED.2005.844739. http://ieeexplore.ieee.org/lpdocs/epic03/wrapper.htm?arnumber=1408167
21. A. Jedaa, M. Burkhardt, U. Zschieschang, H. Klauk, D. Habich, G. Schmid, M. Halik, The impact of self-assembled monolayer thickness in hybrid gate dielectrics for organic thin-film transistors. Org. Electron. **10**(8), 1442–1447 (2009). doi:10.1016/j.orgel.2009.08.006. http://linkinghub.elsevier.com/retrieve/pii/S1566119909002262
22. E.C.P. Smits, S.G.J. Mathijssen, P.a. van Hal, S. Setayesh, T.C.T. Geuns, K.a.H.a. Mutsaers, E. Cantatore, H.J. Wondergem, O. Werzer, R. Resel, M. Kemerink, S. Kirchmeyer, A.M. Muzafarov, S.a. Ponomarenko, B. de Boer, P.W.M. Blom, D.M. de Leeuw, Bottom-up organic integrated circuits. Nature **455**(7215), 956–959 (2008). doi:10.1038/nature07320. http://www.nature.com/doifinder/10.1038/nature07320
23. M.F. Calhoun, J. Sanchez, D. Olaya, M.E. Gershenson, V. Podzorov, Electronic functionalization of the surface of organic semiconductors with self-assembled monolayers. Nat. Mater. **7**(1), 84–89 (2008). doi:10.1038/nmat2059. http://www.ncbi.nlm.nih.gov/pubmed/18026107
24. N. Björklund, F.S. Pettersson, D. Tobjörk, R. Österbacka, Controlling the turn-on-voltage in low-voltage Al2O3 organic transistors with mixed self-assembled monolayers. Synth. Met. **161**(9–10), 743–747 (2011). doi:10.1016/j.synthmet.2011.01.024. http://linkinghub.elsevier.com/retrieve/pii/S0379677911000385

25. U. Zschieschang, M. Halik, H. Klauk, Microcontact-printed self-assembled monolayers as ultrathin gate dielectrics in organic thin-film transistors and complementary circuits. Langmuir **24**(5), 1665–1669 (2008). doi:10.1021/la703818d. http://www.ncbi.nlm.nih.gov/pubmed/18198917
26. P. Stadler, Interfacial Effects in an Organic Semiconductor Heterojunction. Dissertation, Johannes Kepler University Linz, 2011
27. L.-l. Chua, J. Zaumseil, J.-f. Chang, E.C. Ou, General observation of n-type field-effect behaviour in organic semiconductors. Nature **434**(March), 194–199 (2005). doi:10.1038/nature03293.1
28. T.B. Singh, N.S. Sariciftci, Progress in plastic electronics devices. Annu. Rev. Mater. Res. **36**(1), 199–230 (2006). doi:10.1146/annurev.matsci.36.022805.094757. http://arjournals.annualreviews.org/doi/abs/10.1146/annurev.matsci.36.022805.094757
29. Y. Don Park, J.A. Lim, H.S. Lee, K. Cho, Interface engineering in organic transistors. Mater. Today **10**(3), 46–54 (2007). ISSN 1369-7021. http://www.sciencedirect.com/science/article/pii/S1369702107700196
30. H. Ma, H.-L. Yip, F. Huang, A.K.-Y. Jen, Interface engineering for organic electronics. Adv. Funct. Mater. **20**(9), 1371–1388 (2010). doi:10.1002/adfm.200902236. http://dx.doi.org/10.1002/adfm.200902236
31. a. Wang, I. Kymissis, V. Bulovic, a.I. Akinwande, Engineering density of semiconductor–dielectric interface states to modulate threshold voltage in OFETs. IEEE Trans. Electron Devices **53**(1), 9–13 (2006). doi:10.1109/TED.2005.860633. http://ieeexplore.ieee.org/lpdocs/epic03/wrapper.htm?arnumber=1561539
32. X. Sun, C.-a. Di, Y. Liu, Engineering of the dielectric–semiconductor interface in organic field-effect transistors. J. Mater. Chem. **20**(13), 2599 (2010). doi:10.1039/b921449f. http://xlink.rsc.org/?DOI=b921449f
33. Y. Noh, H. Sirringhaus, Ultra-thin polymer gate dielectrics for top-gate polymer field-effect transistors. Org. Electron. **10**(1), 174–180 (2009). doi:10.1016/j.orgel.2008.10.021. http://linkinghub.elsevier.com/retrieve/pii/S1566119908002127
34. J. Cornil, J.-L. Brédas, J. Zaumseil, H. Sirringhaus, Ambipolar transport in organic conjugated materials. Adv. Mater. **19**(14), 1791–1799 (2007). doi:10.1002/adma.200602922. http://doi.wiley.com/10.1002/adma.200602922
35. X.-H. Zhang, B. Domercq, B. Kippelen, High-performance and electrically stable C60 organic field-effect transistors. Appl. Phys. Lett. **91**(9), 092114 (2007). doi:10.1063/1.2778472. http://link.aip.org/link/APPLAB/v91/i9/p092114/s1&Agg=doi
36. X.-H. Zhang, B. Kippelen, Low-voltage C60 organic field-effect transistors with high mobility and low contact resistance. Appl. Phys. Lett. **93**(13), 133305 (2008). doi:10.1063/1.2993349. http://link.aip.org/link/APPLAB/v93/i13/p133305/s1&Agg=doi
37. H. Sirringhaus, Device physics of solution-processed organic field-effect transistors. Adv. Mater. **17**(20), 2411–2425 (2005). doi:10.1002/adma.200501152. http://doi.wiley.com/10.1002/adma.200501152
38. F. Todescato, R. Capelli, F. Dinelli, M. Murgia, N. Camaioni, M. Yang, R. Bozio, M. Muccini, Correlation between dielectric/organic interface properties and key electrical parameters in PPV-based OFETs. J. Phys. Chem. B **112**(33), 10130 (2008). doi:10.1021/jp8012255
39. M.E. Mills, P. Townsend, D. Castillo, S. Martin, A. Achen, Benzocyclobutene (DVS-BCB) polymer as an interlayer dielectric (ILD) material. Microelectron. Eng. **33**(1–4), 327–334 (1997). doi:10.1016/S0167-9317(96)00061-5. http://linkinghub.elsevier.com/retrieve/pii/S0167931796000615
40. W. Ou-Yang, M. Weis, D. Taguchi, X. Chen, T. Manaka, M. Iwamoto, Modeling of threshold voltage in pentacene organic field-effect transistors. J. Appl. Phys. **107**(12), 124506 (2010). doi:10.1063/1.3449078. http://link.aip.org/link/JAPIAU/v107/i12/p124506/s1&Agg=doi
41. W. Ou-Yang, X. Chen, M. Weis, T. Manaka, M. Iwamoto, Tuning of threshold voltage in organic field-effect transistor by dipole monolayer. Jpn. J. Appl. Phys. **49**(4), 04-04 (2010). doi:10.1143/JJAP.49.04DK04. http://jjap.jsap.jp/link?JJAP/49/04DK04/

42. a. Deman, J. Tardy, PMMA–TaO bilayer gate dielectric for low operating voltage organic FETs. Org. Electron. **6**(2), 78–84 (2005). doi:10.1016/j.orgel.2005.03.002. http://linkinghub.elsevier.com/retrieve/pii/S1566119905000108
43. K.P. Pernstich, S. Haas, D. Oberhoff, C. Goldmann, D.J. Gundlach, B. Batlogg, a.N. Rashid, G. Schitter, Threshold voltage shift in organic field effect transistors by dipole monolayers on the gate insulator. J. Appl. Phys. **96**(11), 6431 (2004). doi:10.1063/1.1810205. http://link.aip.org/link/JAPIAU/v96/i11/p6431/s1&Agg=doi
44. H. Klauk, Contact resistance in organic thin film transistors. Solid-State Electron. **47**(2), 297–301 (2003). doi:10.1016/S0038-1101(02)00210-1. http://linkinghub.elsevier.com/retrieve/pii/S0038110102002101
45. T.B. Singh, N. Marjanovic, G.J. Matt, S. Günes, N.S. Sariciftci, A. Montaigne Ramil, A. Andreev, H. Sitter, R. Schwödiauer, S. Bauer, High-mobility-channel organic field-effect transistors based on epitaxially grown C films. Org. Electron. **6**(3), 105–110 (2005). doi:10.1016/j.orgel.2005.03.006. http://linkinghub.elsevier.com/retrieve/pii/S1566119905000145
46. T.B. Singh, N.S. Sariciftci, H. Yang, L. Yang, B. Plochberger, H. Sitter, Correlation of crystalline and structural properties of C60 thin films grown at various temperature with charge carrier mobility. Appl. Phys. Lett. **90**(21), 213512 (2007). doi:10.1063/1.2743386. http://link.aip.org/link/APPLAB/v90/i21/p213512/s1&Agg=doi
47. L.-L. Chua, P.K.H. Ho, H. Sirringhaus, R.H. Friend, High-stability ultrathin spin-on benzocyclobutene gate dielectric for polymer field-effect transistors. Appl. Phys. Lett. **84**(17), 3400 (2004). doi:10.1063/1.1710716. http://link.aip.org/link/APPLAB/v84/i17/p3400/s1&Agg=doi
48. A. Ortiz-Conde, F.J. Garcia Sanchez, J.J. Liou, A. Cerdeira, M. Estrada, Y. Yue, A review of recent MOSFET threshold voltage extraction methods. Microelectron. Reliab. **42**(4–5), 583–596 (2002). doi:10.1016/S0026-2714(02)00027-6. http://linkinghub.elsevier.com/retrieve/pii/S0026271402000276
49. D. Boudinet, G. Le Blevennec, C. Serbutoviez, J.-M. Verilhac, H. Yan, G. Horowitz, Contact resistance and threshold voltage extraction in n-channel organic thin film transistors on plastic substrates. J. Appl. Phys. **105**(8), 084510 (2009). doi:10.1063/1.3110021. http://link.aip.org/link/JAPIAU/v105/i8/p084510/s1&Agg=doi
50. P. Stadler, A.M. Track, M. Ullah, H. Sitter, G.J. Matt, G. Koller, T.B. Singh, H. Neugebauer, N.S. Sariciftci, M.G. Ramsey, The role of the dielectric interface in organic transistors: a combined device and photoemission study. Org. Electron. **11**(2), 207–211 (2010). doi:10.1016/j.orgel.2009.10.017. http://linkinghub.elsevier.com/retrieve/pii/S1566119909003085
51. G. Heimel, I. Salzmann, S. Duhm, J.A.P. Rabe, N. Koch, Intrinsic surface dipoles control the energy levels of conjugated polymers. Adv. Funct. Mater. **19**(24), 3874–3879 (2009). doi:10.1002/adfm.200901025. http://doi.wiley.com/10.1002/adfm.200901025
52. A. Rajagopal, C.I. Wu, A. Kahn, Energy level offset at organic semiconductor heterojunctions. J. Appl. Phys. **83**(5), 2649 (1998). doi:10.1063/1.367027. http://link.aip.org/link/JAPIAU/v83/i5/p2649/s1&Agg=doi
53. H. Vázquez, W. Gao, F. Flores, A. Kahn, Energy level alignment at organic heterojunctions: role of the charge neutrality level. Phys. Rev. B **71**(4), 1–4 (2005). doi:10.1103/PhysRevB.71.041306. http://link.aps.org/doi/10.1103/PhysRevB.71.041306
54. K. Sakamoto, Electronic structure of K-doped C60 monolayer films adsorbed on Si(0 0 1)-(2x1) and Si(1 1 1)-(7x7) surfaces. Surf. Sci. **499**(1), 63–72 (2002). doi:10.1016/S0039-6028(01)01794-0. http://linkinghub.elsevier.com/retrieve/pii/S0039602801017940
55. C. Cepek, P. Schiavuta, M. Sancrotti, M. Pedio, Photoemission study of C 60 / Si (111) adsorption as a function of coverage and annealing temperature. Phys. Rev. B **60**(3), 2068–2073 (1999). doi:10.1103/PhysRevB.60.2068. http://link.aps.org/doi/10.1103/PhysRevB.60.2068
56. M.W. Ruckman, B. Xia, S.L. Qiu, Adsorption of C60 on Ta(110): photoemission and C K-edge studies. Phys. Rev. B **48**(20), 15457 (1993)
57. S.J. Chase, W.S. Bacsa, M.G. Mitch, L.J. Pilione, J.S. Lannin, Surface-enhanced Raman scattering and photoemission of C60 on noble-metal surfaces. Phys. Rev. B **46**(12), 7873–7877 (1992)

58. J. Ivanco, F.P. Netzer, M.G. Ramsey, On validity of the Schottky–Mott rule in organic semiconductors: sexithiophene on various substrates. J. Appl. Phys. **101**(10), 103712 (2007). doi:10.1063/1.2734879. http://link.aip.org/link/JAPIAU/v101/i10/p103712/s1&Agg=doi
59. W. Osikowicz, M.P. de Jong, W.R. Salaneck, Formation of the interfacial dipole at organic-organic interfaces: C60/Polymer interfaces. Adv. Mater. **19**(23), 4213–4217 (2007). doi:10.1002/adma.200700622. http://doi.wiley.com/10.1002/adma.200700622
60. S. Braun, W. Osikowicz, Y. Wang, W.R. Salaneck, Energy level alignment regimes at hybrid organic–organic and inorganic–organic interfaces. Org. Electron. **8**(1), 14–20 (2007). doi: 10.1016/j.orgel.2006.10.006. http://linkinghub.elsevier.com/retrieve/pii/S156611990600142X